FOSSEE, IIT Bombay
OpenFOAM Case Study Project
August, 2023

The Effect of Flexible Flaps on the flow dynamics of a Stalled Airfoil

Sambhav Sahani[1] and Chandan Bose[2]

[1]UG Research Scholar, Dept. of Mechanical and Aerospace Engineering, Tribhuvan University, IOE, Pulchowk Campus
[2]Assistant Professor, Aerospace Engineering, School of Metallurgy and Materials, The University of Birmingham

August 30, 2023

Synopsis

The operational limit of Micro Aerial Vehicles (MAVs) can be extended by delaying flow separation using biomimetic methodology inspired by secondary covert feathers of a bird's wings that appear on the upper surface during high angle-of-attack manoeuvres or sudden gusts. This is canonically modelled as a flexible flap on the upper surface of an airfoil in the present study. This study sets up a case for fluid-structure interaction (FSI) simulation of a flexible flap on the surface of a NACA0012 airfoil at an angle-of-attack of 45° and Reynolds Number of 1000. The present open-source FSI framework comprises a finite volume method based incompressible flow solver 'pimpleFoam' available in OpenFOAM, a finite element method based structural solver CalculiX, and a coupling platform preCICE. A parallel-implicit scheme is used with the nearest neighbour mapping technique for coupling the fluid and the solid solvers. Three different flap positions (10% chord, 50% chord, and 90% chord) were studied. Among the three, comparing the mean drag coefficient ($\overline{C_d}$), flap at 90% chord was found to be the most aerodynamically efficient. However, to get the optimal position of the flap, a systematic study has to be conducted comparing various flap positions in terms of generated lift and mean lift-drag ratio, among others.

1 Introduction

Micro Aerial Vehicles (MAVs) are a class of Unmanned Aerial Vehicles (UAVs) having dimensions less than 15cm in every direction. Their flight regimes are also characterized by low Reynolds numbers [1]. Due to their high flight efficiency, high manoeuvrability, and low flight noise, their popularity is rising, with applications in Search and Rescue (SAR) missions, environmental protection, photography, and more. Control of boundary layer separation is one of the important challenges in designing MAVs due to their operational requirements, which include being agile enough to move

around sharp corners and bends [2]. One of the biomimetic methodologies being studied for separation control is inspired by secondary covert feathers that pop up during landing or sudden increase of angle of attack due to gusts on the upper surface of bird wings, as shown in figure 1. According to Liebe [3] and Carruthers et al. [4], these covert feathers delay flow separation with increasing angle of attack and thus contribute to higher lift.

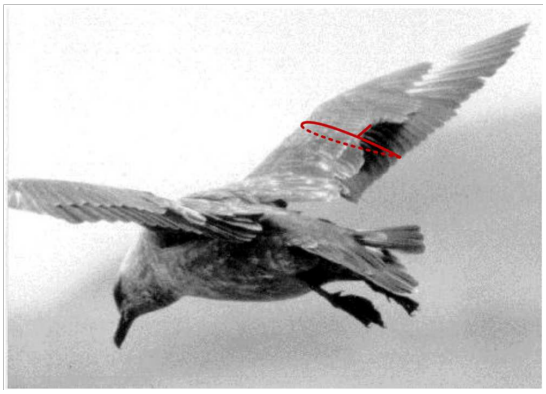

Figure 1: Popped up secondary covert feathers [2].

In futuristic MAV designs, these covert feathers can be modelled as a flap on the upper surface of the wings. Many numerical and experimental studies have been carried out to characterize the effectiveness of using such flaps. Kernstine et al. [5] studied the effect of the flap size, chord placement, configuration, and material on the flow dynamics of a NACA 2412 airfoil. The authors also studied how the flow Reynolds number would affect these configurations. Using Direct Numerical Simulation (DNS), Rosti et al. [6] studied the underlying physics of the flow over NACA 0020 airfoil at an AOA of 20° with and without a flexible flap over it. According to the preliminary optimization done by them to finalize a quasi-optimal flap configuration, it is of fundamental importance to lock-in the flap oscillation frequency with the associated Strouhal frequency. Fang et al. [2] varied the length, position, bending coefficient ($k^* = EI/(\rho_f U_\infty^2 L^3)$, and mass ratio ($M^* = \rho_s h/\rho_f L$) of the flap to obtain optimal flap configuration for NACA0012 airfoil at 10° AOA, and a Reynolds number of 1000. However, a detailed study to characterize the effect of length, aspect ratio, position, material, number of flaps, and flow Reynolds number in high angle of attack region like 45° is missing in the existing literature. The present study attempts to set up a case that can be used to study the effect of a flexible flap's various properties in post-stall conditions.

Fluid-structure interaction (FSI) problems, like the present one, can be solved using either monolithic or partitioned approaches. In a monolithic approach, a single solver is set up that can handle both the fluid dynamic and the structural dynamic equations. In a partitioned approach, different solvers are used to solve the fluid dynamic and the structural dynamic equations separately, and a coupling mechanism is used to transfer the fluid force to the solid solver, which then calculates the deformation and passes it back to the fluid solver. Different methods can be used to handle the individual components within the partitioned approach; for example, Fang et al. [2] used Lattice Boltzmann Method (LBM) for Fluid, Finite Element Method (FEM) for Solid, and Immersed Boundary Method (IBM) to handle the interaction between fluid and solid. However, the common

(and readily available) approach to solving FSI problems is using Finite Volume Method (FVM) for fluid, Finite Element Method (FEM) for solid, and exchanging information between them using a coupling mechanism. preCICE is an open-source software package that enables the coupling of separate solvers for different types of numerical models [7]. Different FSI benchmark cases like Turek & Hron FSI, pulsating flow over a flexible flap have been validated using preCICE [8]. Along with preCICE, open-source software OpenFOAM (FVM) and CalculiX (FEM) can be used to handle the fluid and the solid dynamics, respectively, thus, completing the FSI setup using a completely open-source framework.

The primary objective of this project is to set up the FSI case of a thin, flexible flap on an airfoil using OpenFOAM, CalculiX, and preCICE. This setup can be used in further studies, varying the solid and the fluid models as needed. The secondary objectives of this project are to study the effects of the flexible flap on the flow dynamics and to study how the variation of the position of the flap would affect its aerodynamic characteristics. It must, however, be noted that this short report provides the details of the FSI framework and extensive validation of the model is yet to be achieved in the future.

The remaining report consists of three major sections. Section 2, Governing Equations and Models, defines the problem, establishes the necessary governing equations, provides an overview of the geometry and the mesh, and details the solver setup. Section 3 goes over the results. This section interprets the results of the domain size, grid size, and time-step size convergence studies. Also, the effect of the flexible flap on the flow dynamics and the flap position's effect on the airfoil's aerodynamic characteristics are discussed here. The final section provides a conclusion of the study.

2 Governing Equations and Models

2.1 Problem definition

This study investigates the effect of flexible flaps on the flow dynamics of a stalled NACA0012 airfoil. A representative geometry of the problem is shown in Figure 2. For post-stall study, the angle of attack (α) of the airfoil must be greater than the critical angle of attack (α_{cric}). The flap position is varied (10% chord, 50% chord, and 90% chord) to characterize its effect on the aerodynamic performance. The Reynolds number of the flow is set to 1000, which lies within the operational range of MAVs.

2.2 Governing equations

Three sets of equations govern the fluid, the structure, and the fluid-structure interface part of this problem.

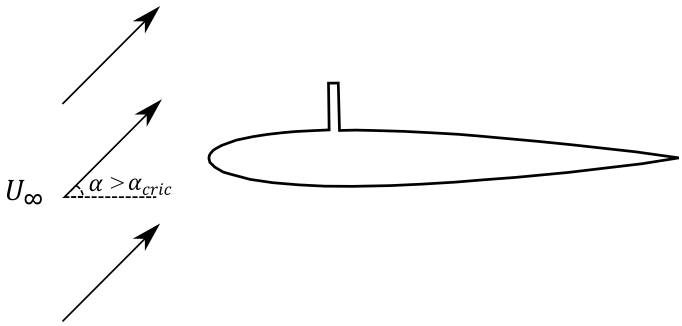

Figure 2: Geometry of the airfoil with a flexible flap.

2.2.1 Fluid

Within the OpenFOAM framework, pimpleFoam, a transient, incompressible solver based on the PIMPLE algorithm, is used. As the flow is in the laminar regime, no turbulence model is required.

Unsteady, incompressible, two-dimensional flows are governed by the following sets of equations.

Continuity Equation:

$$\nabla \cdot \mathbf{u} = 0 \tag{1}$$

Momentum Equation:

$$\frac{\partial \mathbf{u}}{\partial t} + \mathbf{u} \cdot (\nabla \cdot \mathbf{u}) = -\frac{1}{\rho}(\nabla \cdot p) + \nu \nabla^2 \cdot \mathbf{u} \tag{2}$$

where,

ρ is the density,

ν is the kinematic viscosity

u is the velocity vector,

f is the force vector, and

p is the pressure.

2.2.2 Structure

The time-dependent von Kármán plate equation, expressed below, governs the structure.

$$\rho_s h_s \frac{\partial^2 W}{\partial^2 t} + \frac{E h_s^3}{12(1-\nu^2)} \Delta^2 W = f_{ext} \tag{3}$$

where,

Δ is the Poisson operator,

w is the vertical deflection,

h_s is the thickness,

ρ_s is the solid's density,

E is the Young's modulus,

ν is the Poisson's ratio, and

f_{ext} is the net external force per unit length in the vertical direction.

.

For a single beam element, the Finite Element Method (FEM) equation can be written as:

$$M\ddot{w} + \bar{D}\dot{w} + Kw = f \tag{4}$$

where,

M is the Mass Matrix,

D is the Damping Matrix,

K is the Stiffness Matrix, and

f is the Force Matrix.

2.2.3 Fluid-Structure Interface

For a two-way coupled FSI simulation, the following two sets of equations/conditions must be satisfied in the fluid-solid interface:

Kinematic Coupling Condition, which ensures that both the fluid and structural part have the same displacement, and velocity at the fluid-structure interface.

$$x_f = w_s \tag{5}$$

$$v_f = \frac{\partial w_s}{\partial t} \tag{6}$$

Dynamic Coupling Condition, which ensures that the stress or force is balanced at the fluid-structure interface.

$$\sigma_f \cdot n_f = -\sigma_s \cdot n_s \tag{7}$$

where,

x_f is the deformation at the interface in the fluid domain,

w_S is the deformation at the interface in the structural component,

v_f is the fluid velocity at the interface,

σ is the stress, and

n is the normal.

2.3 Geometry and Mesh

The representative geometry of the problem is already shown in figure 2. A flap of length 0.1c (chord length) with an aspect ratio of 15 is used in this study. The flap is placed at three different locations, 0.1c, 0.5c, and 0.9c, to study the effect of the variation of the flap position.

The domain size has been selected by conducting a domain size independence study, as will be discussed in Section 3.1.1. As per the study, the result obtained from the domain, which extends -9c to 20c along the x-axis and -9c to 9c along the y-axis is domain size independent. It must be noted that the coordinates have been mentioned with the origin at the leading edge of the airfoil.

To finalize the grid size for fluid and solid mesh, a grid size convergence test has been done, as will be discussed in Section 3.1.2. The converged fluid mesh has 110866 hexahedral cells, and the converged solid mesh has 237 quadrangles. Figure 4 shows the converged fluid and solid mesh, respectively.

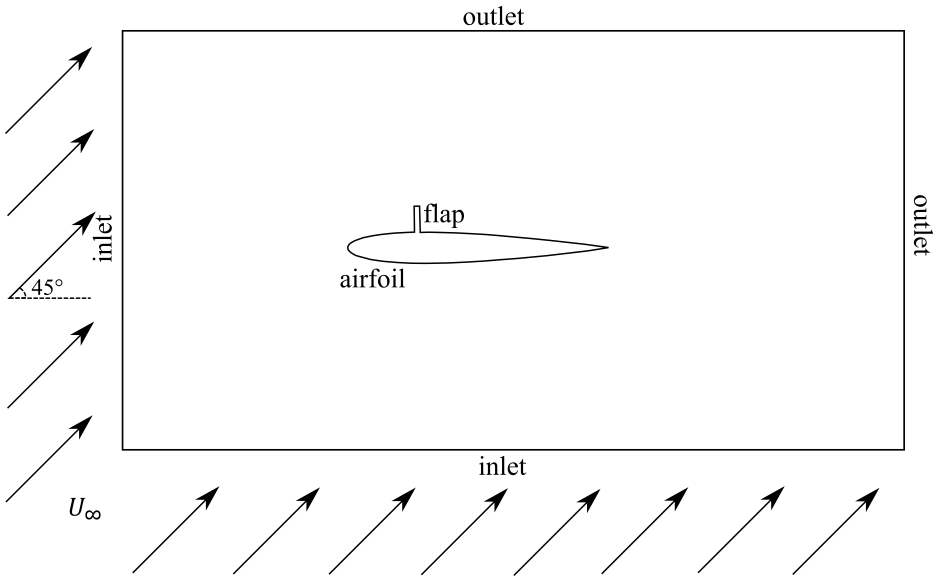

Figure 3: Problem definition and the computational domain.

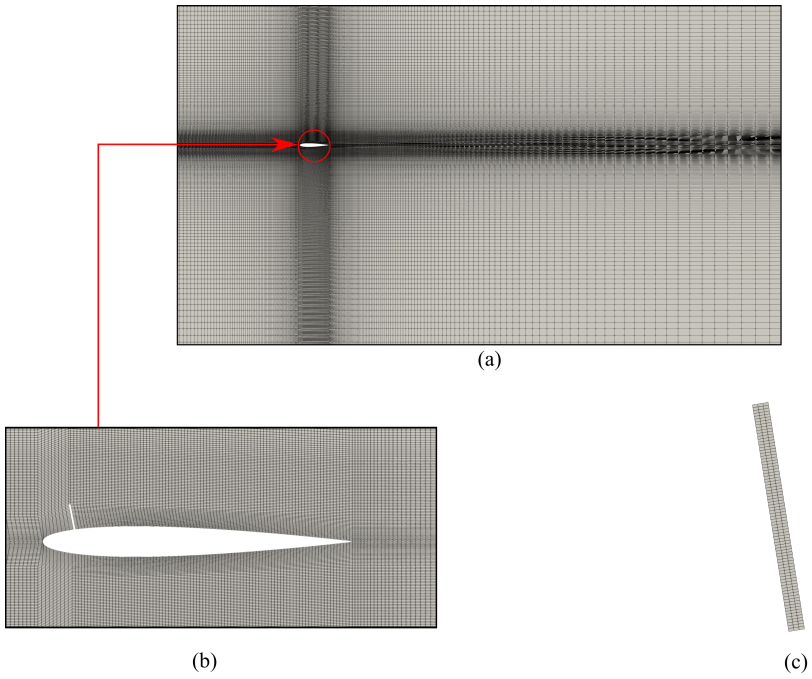

Figure 4: (a) Fluid mesh, (b) fluid mesh near the airfoil surface, (c) solid mesh.

2.4 Solver setup

The overall setup can be divided into three parts: fluid setup, structure setup, and coupling setup.

2.4.1 Fluid Setup

2.4.1.1 Initial and Boundary Conditions

The free stream velocity is taken to be 0.05 m/s, and the a Reynolds number of 1000 is going to be maintained by adjusting the value of kinematic viscosity for the fixed value of airfoil chord length. As the airfoil is at an angle of attack with the incoming free stream, the velocity at the domain inlet is resolved along the x-direction and the y-direction as follows:

$$u = U_\infty \cos(\alpha), \tag{8}$$

$$v = U_\infty \sin(\alpha), \tag{9}$$

where u and v are free stream velocity (U_∞) components along the x and y directions respectively.

The boundary conditions at all the patches are tabulated in Table 1.

Table 1: Boundary Conditions

Patch	Velocity	Pressure	Point Displacement
Inlet	fixedValue	zeroGradient	fixedValue
Outlet	zeroGradient	fixedValue	fixedValue
Airfoil	noSlip	zeroGradient	fixedValue
Flap	movingWallVelocity	zeroGradient	fixedValue

2.4.1.2 Fluid Properties

The kinematic viscosity (ν) of the fluid can be calculated using the following relation of Reynolds Number (Re):

$$Re = \frac{Ul}{\nu}. \tag{10}$$

Here, l denotes the characteristics length which is the chord length of the airfoil. As the values of Re, U, and l are known, ν can be easily calculated. For the current study with Re = 1000, U = 0.05 m/s, l = chord length = 1 m, the value of ν becomes 5.025×10^{-5} m^2s^{-1}. As the flow Reynolds number is in the laminar range, no turbulence model has been used.

2.4.1.3 Dynamic Mesh Treatment

To update the mesh with the deflection of the flap, mesh morphing approach is used in OpenFOAM. To handle the mesh morphing, displacementLaplacian solver is used within which quadratic inverseDistance method is selected.

2.4.1.4 Finite Volume Schemes

Table 2: Finite Volume Schemes

Operation	Scheme
Time Derivative	Euler
Gradient	Gauss linear
	default none
Divergence	div(phi,U) bounded Gauss upwind
	div((nuEff*dev2(T(grad(U))))) Gauss linear
Laplacian	Gauss linear corrected
Surface Normal Gradient	corrected
Interpolation	linear

2.4.1.5 Solution Method and Control

A preconditioned Conjugate Gradient (PCG) solver is used for pressure with a Diagonal-based Incomplete Cholesky (DIC) preconditioner. smoothSolver with symGaussSeidal smoother is used

to solve velocity and cell displacement. Four correction steps are used within a single time-step and one non-orthogonal corrector is used. Flow time-step of 10^{-3} s is selected.

2.4.2 Structure Setup

2.4.2.1 Boundary Conditions

The bottom face of the flap, attached to the airfoil surface, has no translational degree of freedom. All other faces are limited in translation in the third direction (z-axis), and the force from the fluid solver is applied to these faces.

2.4.2.2 Material Properties

The material properties of the solid used in this study are as follows:

Density = $3000 kg/m^3$

Young's Modulus = 1 MPa

Poisson's Ratio = 0.3

2.4.2.3 Control

Time step of 10^{-3} s is used.

2.4.3 Coupling Setup

Within the partitioned approach of two-way FSI, there can be two further different approaches: weak coupling and strong coupling. Weak coupling is also known as explicit coupling, and strong coupling is also known as implicit coupling. In implicit coupling, multiple iterations are done within a single coupling timestep to satisfy the dynamic and kinematic coupling conditions. In explicit coupling, only a single iteration is done without regard for dynamic and kinematic coupling conditions. In FSI cases like this, where the deflection is large, implicit coupling is a better approach as the accumulated error becomes too significant in explicit coupling. Both approaches were tested in the current study with the explicit coupling approach leading to solver crashes. Hence, the implicit coupling approach is chosen. An overview of the coupling setup is shown in Figure 5. As can be seen in the figure, a parallel-implicit coupling scheme is used with a first-order mapping scheme, nearest-neighbor. For acceleration, Interface Quasi-Newton Inverse Least Squares (IQN-ILS) scheme is used, which is a good choice for strong interactions. Coupling time-step of 10^{-3} s is used.

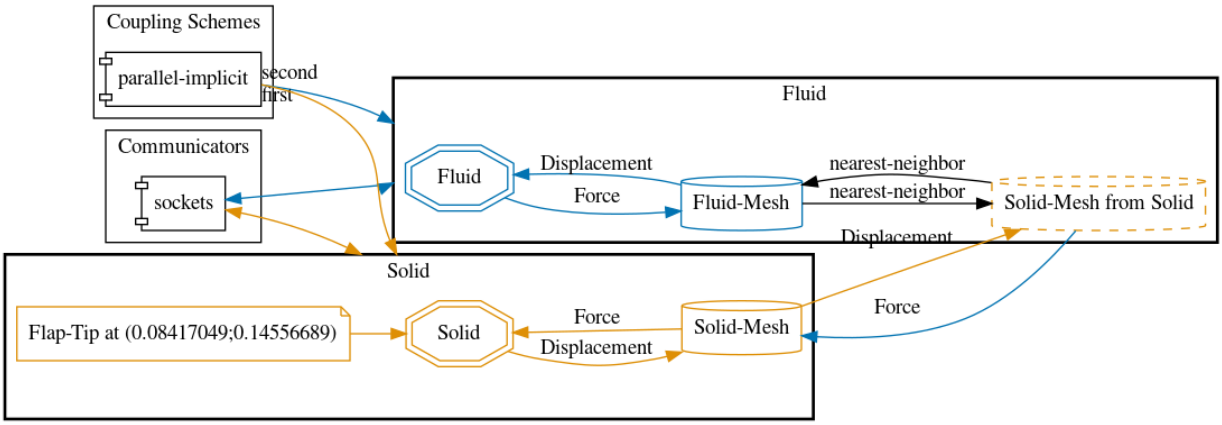

Figure 5: Flow chart of the coupling algorithm.

3 Results and Discussions

3.1 Convergence Tests

3.1.1 Domain Size Convergence Test

Three different domain sizes were considered to conduct the domain size convergence test. The dimensions of the tested geometry are mentioned in Table 3. Here, c refers to the chord length of the airfoil. The deformation history of the left flap tip for the three different domain sizes are shown in figure 6. A comparison is made between the three domains based on the value of the mean drag coefficient ($\overline{C_d}$). Figure 7 shows the value of $\overline{C_d}$ for the three domain sizes. As the relative percentage error between domains 2 and 3 is just 2.038 %, domain 2 is selected for further study.

Table 3: Domain Sizes

Domain	X Range	Y Range
1	-6c to 15c	-6c to 6c
2	-9c to 20c	-9c to 9c
3	-12c to 25c	-12c to 12c

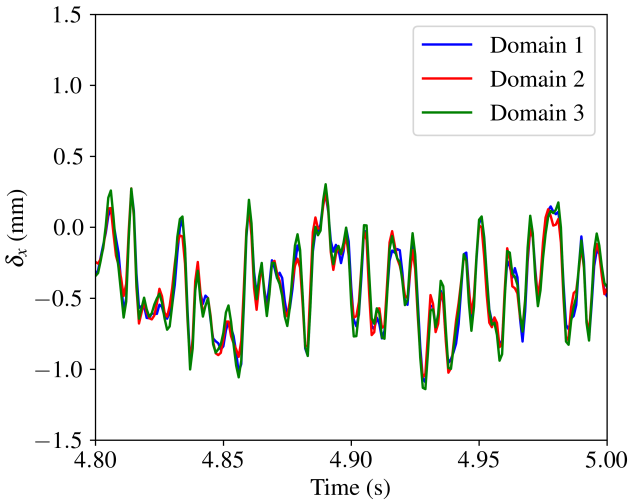

Figure 6: Flap tip displacement time history.

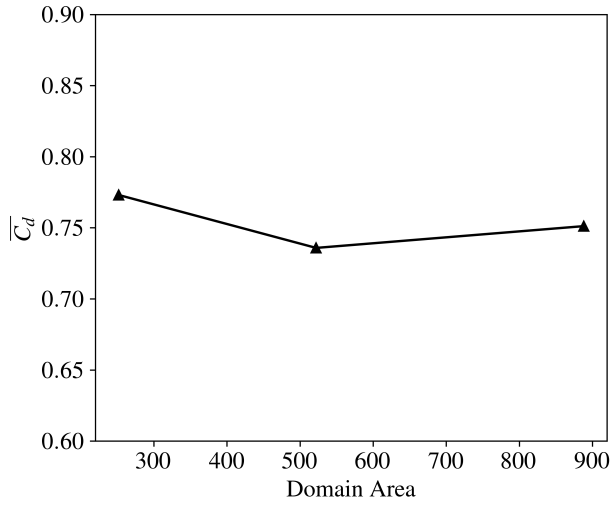

Figure 7: Comparison of mean drag coefficient.

Table 4: Relative Percentage Error of $\overline{C_d}$

Domain	Relative Percentage Error
1 - 2	-5.056 %
2 - 3	2.038 %

3.1.2 Grid Size Convergence Test

Three sets of solid and fluid mesh were used to conduct the grid size convergence test. The number of cells in the fluid and solid mesh corresponding to each test is given in Table 5.

Table 5: Number of Cells

Mesh	Number of Cells in Fluid Domain	Number of Cells in Solid
1	55916	112
2	110866	237
3	225118	565

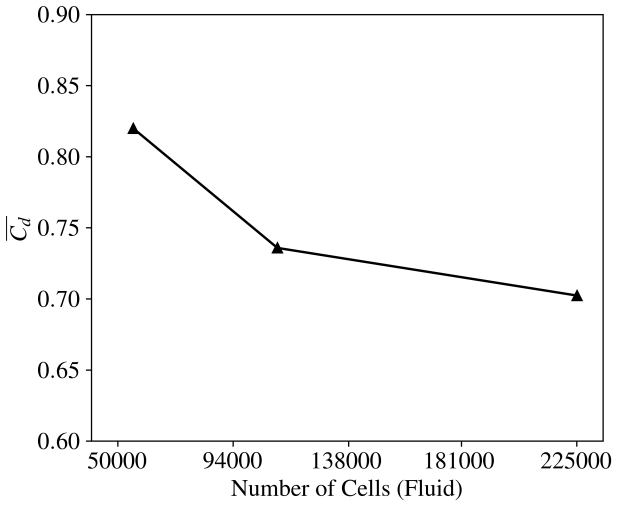

Figure 8: Comparison of mean drag coefficient.

Table 6: Relative Percentage Error of $\overline{C_d}$

Mesh	Relative Percentage Error
1 - 2	-11.422 %
2 - 3	-4.772%

The variation of the value of $\overline{C_d}$ with the change in grid size is shown in figure 8, and the relative percentage error between the different grid sizes are shown in Table 6. Based on this, mesh 2, with a relative percentage error of less than 5%, is selected.

3.1.3 Time Step Convergence Test

The time steps of the fluid and the solid solver, and the coupling time step between them are kept the same throughout this study. For the time step convergence test, three time steps, 10^{-2} s, 10^{-3} s, and 10^{-4} s, are taken.

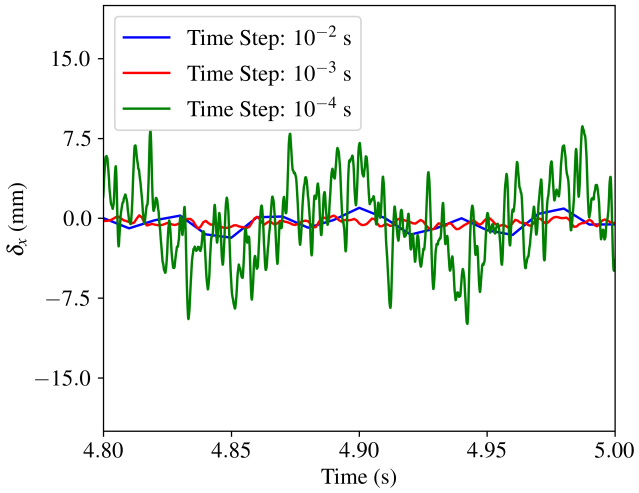

Figure 9: Flap tip displacement time history.

Looking at Figure 9, it is clear that time steps of 10^{-2} s, and 10^{-3} s are unable to capture the displacement as predicted by the time step of 10^{-4} s. But as the scope of this study is just limited to using OpenFOAM, CalculiX, and preCICE to run FSI simulation of thin flexible flaps without much regard to getting a very accurate solution with the limited computational resources available, the time step of 10^{-3} s is chosen for further study.

3.2 Flexible flap and Flow Dynamics

To understand how the flexible flap affects the flow dynamics and what effects the flow has on the flap, flap at 10% chord location is studied. A comparison will be made in the subsequent section on how the position of the flap affects the aerodynamic performance of the airfoil.

As can be seen in the pressure contour in Figure 10 (a), alternate regions of high and low pressure can be seen on (and around) the surface of the flap on both sides, high-pressure area on one side, accompanied by low-pressure region on the corresponding another side. The motion of the flap is driven by these alternating regions of positive and negative pressure differences (taking any direction as positive or negative), giving it a wavy profile, as can be seen in Figure 11.

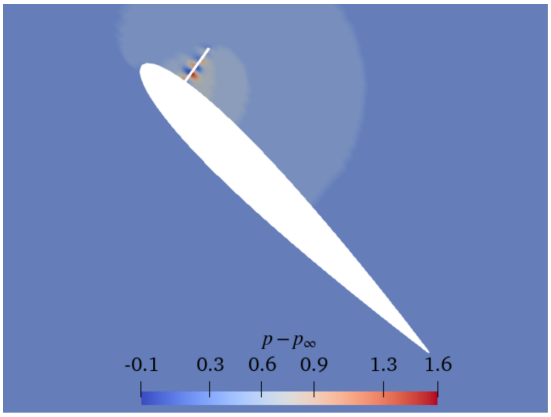

(a)

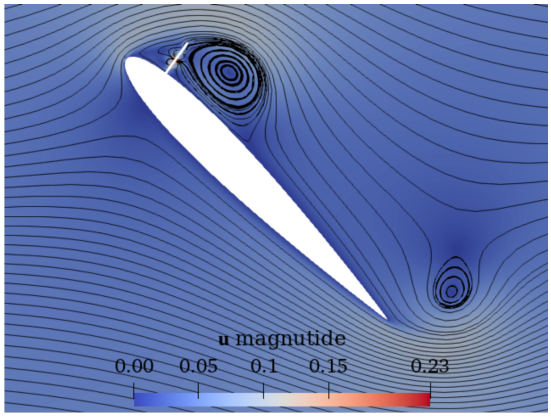

(b)

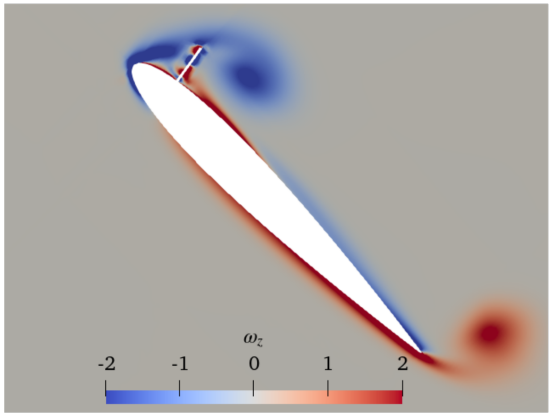

(c)

Figure 10: (a) Pressure contour, (b) velocity contour, and (c) vorticity contour around the foil with a flexible flap.

The clockwise and anticlockwise vortices generated around the airfoil can be visualized in the velocity and vorticity contours as shown in Figure 10 (b), and 10 (c), respectively. Vortices of different strengths and directions can be seen around the flap. These vortices are responsible for the pressure fluctuations and differences on the flap surface, which in turn drive the flap's deformation.

The deflection of the flap, as shown in Figure 11, is too small for the magnitude of pressure and vortices generated. This was expected as the coupling time used is 10^{-3} s. The peak displacement of the flap's left tip, as predicted by coupling time of 10^{-4} s, is 18.05 times the peak predicted by coupling time of 10^{-3} s.

Comparison of Fast Fourier Transform (FFT) of the two time steps, as shown in Figure 12, shows that, although the dominant frequency lies within the range for both the coupling times, coupling time of 10^{-4} s is able to capture the magnitude better. Hence, as mentioned already, the results presented here are not accurate and are a demonstration of OpenFOAM, CalculiX, and preCICE's ability to perform FSI simulation of such thin flaps. For a proper simulation of the current case, a lower coupling timestep is required, or the materials of the flap and the flow properties have to be

selected such that the coupling timestep used is justified.

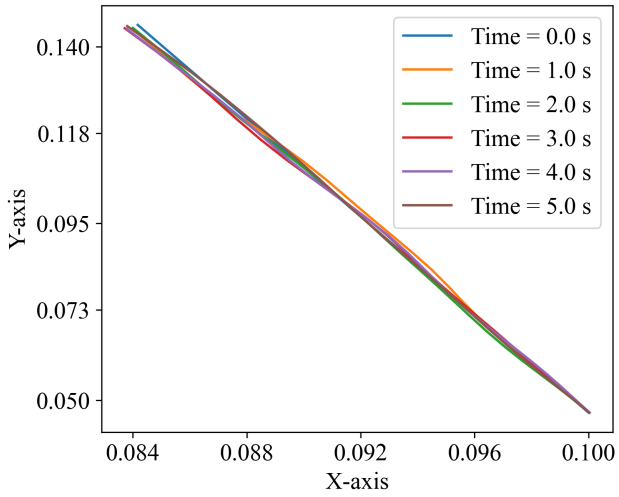

Figure 11: Deflection envelope of the flexible flap.

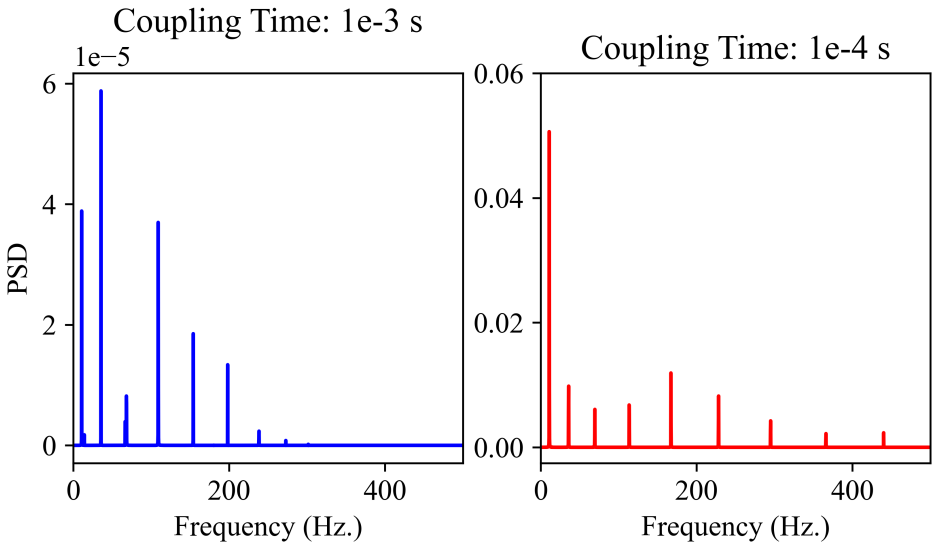

Figure 12: Frequency spectra of the flap's tip displacement.

3.3 Flap's Position and Aerodynamic Characteristics

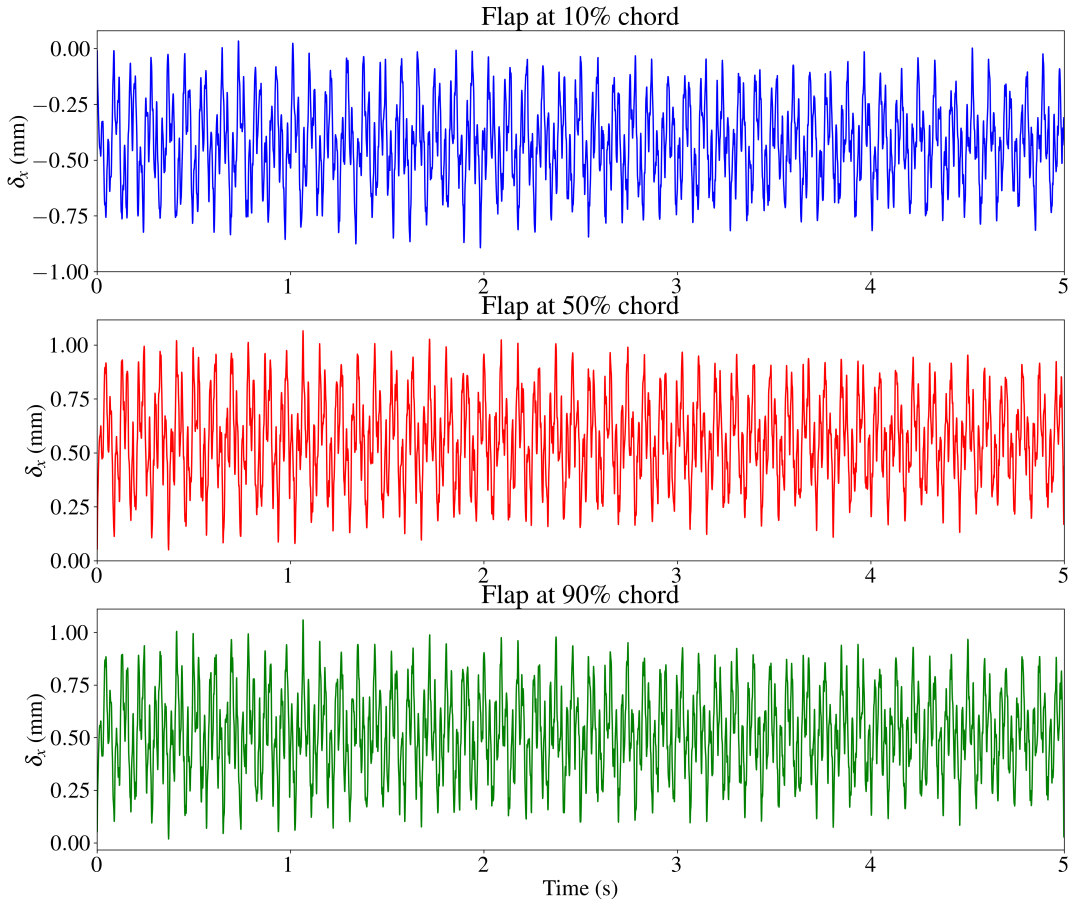

Figure 13: Time histories of the tip displacement of the flexible flap for different flap locations.

The deformation history of the flap's tip for the three different flap positions can be seen in Figure 13. It can be observed that the flap at 10% chord deflects to the left and the flap at 50% and 90% chord deflect towards the right in the simulated time frame. This is related to the suction strength of the vortices formed. As can be seen in Figure 10 (c), 14 (a), and 14 (b), the flap is under the influence region of the upstream vortex for the 10% chord case, while, for the 50% and the 90% chord case, the upstream vortex has not yet reached the flap. Because of this, the flap's deflection is dominated by the upstream vortex's suction for the 10% case, and (flap's) downstream vortex's suction for the 50% and 90% case.

This may however change as the simulation is run for a longer duration, and all the flaps come under the influence region of the upstream vortex. Then the flap's deflection would be a result of the struggle between the upstream and the downstream vortex's suction, the flap deflecting more in

whichever direction has higher strength.

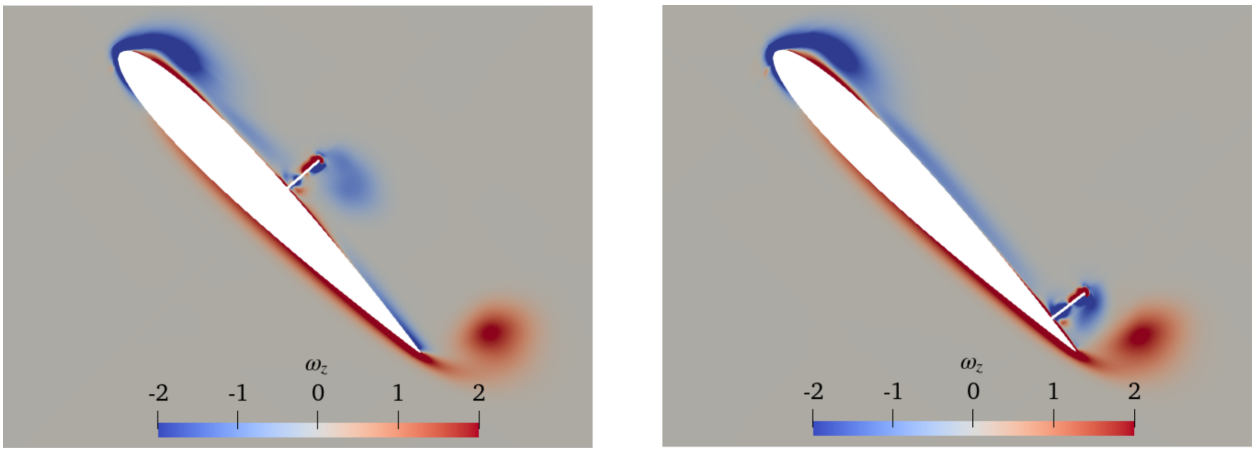

(a) (b)

Figure 14: Vorticity contours: the flexible flap at (a) 50% chord, (b) 90% chord.

Table 7: Drag Coefficient Comparison

Flap Position (x/c)	0.1	0.5	0.9
Mean Drag Coefficient ($\overline{C_d}$)	0.74	0.24	0.15

The mean drag coefficient ($\overline{C_d}$) of three different flap positions are compared in Table 7. Comparing just the value of $\overline{C_d}$, with the limited data available, the flap near the trailing edge of the airfoil appears to be most aerodynamically favorable. However, more flap positions have to be simulated for a longer flow duration to pinpoint the optimal position.

3.3.1 Fluid-Structure Interaction and Reference Pressure

The flap's deformation is (obviously) affected by the reference pressure used. This study used 1.01×10^5 Pascal (or $1.01 \times 10^5/\rho_f$ kinematic pressure) as the reference pressure. Hence, the load in the flap is large (considering the nature of the problem), and thus, the material properties of the flap had to be selected such that this extreme load would not deflect the flap by extreme amounts. Even after selecting proper material properties, there is a huge imbalance between the net load acting on one of the sides of the flap and the net load acting on the upper flap surface as the loads on the sides are balanced. Still, no external load is present to balance the load in the upper face. Because of this, the flap has a deformation profile where the deformation of the middle portion of the flap is comparable with the upper portion. This would not have been the case if the load was not very large in the upper face. The flap's upper face would have led the deflection with all the other sections below it following it. To get the desired nature of the flap's deformation, a balance must have been found between the extreme loads and the material properties, which, unfortunately, could not be done within this study. However, a reference pressure of 0 Pascal would have provided

more flexibility in choosing the material properties, allowing lower values of Young's Modulus and Density. Hence, for a numerical study, the reference pressure should be appropriately chosen depending on the physics of the problem and the nature of the deformation desired.

4 Conclusions

The setup of a case for FSI simulation of a flexible flap on the upper surface of a stalled NACA0012 airfoil at an AOA of 45° and a Reynolds Number of 1000 using OpenFOAM (FVM), CalculiX (FEM) and preCICE has been completed. However, validation of the fluid setup, as well as the overall FSI setup, has yet to be done, and the results should be interpreted as such. As per the time step convergence study conducted, a coupling timestep of 10^{-4} s (or higher) is required for the current fluid and solid properties. Due to the computational and time constraints, the time step of 10^{-3} s is used. For an accurate study, the proper converged time step must be used, or the fluid and solid properties must be selected to justify the used time step. The flap at three different positions, 10% chord, 50% chord, and 90% chord, have been studied. The comparison of the mean drag coefficient among the three positions showed that the flap near the trailing edge (90% chord) was the most aerodynamically favourable. However, to get the flap's optimal position, a detailed study has to be conducted comparing more flap positions and other aerodynamic coefficients like mean lift, mean lift-drag ratio, maximum lift fluctuation, and maximum drag fluctuation. Also, the deflection of the flap is dominated by the strength of the suction of the flap's upstream and downstream bubbles. Hence, simulation of longer flow duration is required such that the flap is in the range of influence of the upstream separation bubble.

5 Acknowledgement

First and foremost, I extend my heartfelt gratitude to Dr. Chandan Bose, my supervisor, whose valuable insights and guidance from the project's inception to completion were instrumental in its successful completion and provided me with a significant learning opportunity. This project would not have been possible without him. I would also like to thank Mr. Aabhusan Regmi for all of his invaluable technical assistance. Having the opportunity to learn from Prof. Manaswita Bose's insights during the weekly review meeting was a significant benefit of this fellowship. Last but definitely not least, I'd like to thank Mrs. Payel Mukherjee, the FOSSEE team, and IIT Bombay for providing the opportunity, resources, and support that were critical to the project's success.

References

[1] J. Hall and K. Mohseni, *Micro Aerial Vehicles*. Boston, MA: Springer US, 2013, pp. 1–10. [Online]. Available: https://doi.org/10.1007/978-3-642-27758-0_892-2

[2] Z. Fang, C. Gong, A. Revell, G. Chen, A. Harwood, and J. O'connor, "Passive separation control of a naca0012 airfoil via a flexible flap," *Physics of Fluids*, vol. 31, no. 10, p. 101904, 2019.

[3] W. Liebe, "Der auftrieb am tragflügel: Entstehung und zusammenbruch," *Aerokurier*, vol. 12, no. 1520, p. 54, 1979.

[4] A. C. Carruthers, A. L. Thomas, and G. K. Taylor, "Automatic aeroelastic devices in the wings of a steppe eagle aquila nipalensis," *Journal of Experimental Biology*, vol. 210, no. 23, pp. 4136–4149, 2007.

[5] K. Kernstine, C. Moore, A. Cutler, and R. Mittal, "Initial characterization of self-activated movable flaps," pop-up feathers"," in *46th AIAA Aerospace Sciences Meeting and Exhibit*, 2008, p. 369.

[6] M. E. Rosti, M. Omidyeganeh, and A. Pinelli, "Numerical simulation of a passive control of the flow around an aerofoil using a flexible, self adaptive flaplet," *Flow, Turbulence and Combustion*, vol. 100, pp. 1111–1143, 2018.

[7] G. Chourdakis, K. Davis, B. Rodenberg, M. Schulte, F. Simonis, B. Uekermann, G. Abrams, H. Bungartz, L. Cheung Yau, I. Desai, K. Eder, R. Hertrich, F. Lindner, A. Rusch, D. Sashko, D. Schneider, A. Totounferoush, D. Volland, P. Vollmer, and O. Koseomur, "preCICE v2: A sustainable and user-friendly coupling library [version 2; peer review: 2 approved]," *Open Research Europe*, vol. 2, no. 51, 2022. [Online]. Available: https://doi.org/10.12688/openreseurope.14445.2

[8] G. Chourdakis, D. Schneider, and B. Uekermann, "Openfoam-precice: Coupling openfoam with external solvers for multi-physics simulations," *OpenFOAM® Journal*, vol. 3, pp. 1–25, 2023.